Ground-Based Water Vapor Retrieval in Antarctica: An Assessment

Monia Negusini, *Member, IEEE*, Boyan H. Petkov, Pierguido Sarti, and Claudio Tomasi

***Abstract*—The atmospheric water vapor is an important indicator of the Earth's climate state and evolution. We therefore aimed at calculating the content and long-term variation of the precipitable water vapor at five coastal Antarctic stations, i.e., Casey, Davis, Mawson, McMurdo, and Mario Zucchelli. To do that, we processed the 12-year time series of GPS and radiosounding (RS) observations acquired at those stations, with the purpose of ensuring the utmost accuracy of the results adopting homogeneous, consistent, and up-to-date processing strategies for both data sets. Using the two fully independent techniques, rather consistent contents and seasonal variations of precipitable water were detected, mainly ranging from 1 (Austral winter) to 10 mm (Austral summer). At each site, correlation coefficients varying from 0.86 to 0.91 were found between the GPS and RS time series, with mean discrepancies $\leq$0.75 mm. There is no clear indication regarding the possible dry or wet biases of one technique with respect to the other, with only a notable GPS wet bias identified at Mawson and a dry bias at Casey that, nevertheless, correspond to an average difference of $<$ 1 mm on the two series; the biases at the other sites are much smaller. Although extremely small, i.e., ranging from $-$0.03 to 0.04 mm/year, the linear trends of the series are not always consistent in sign. In accordance with the major climate models, the RS linear trends are mostly positive, whereas depending on the site, GPS exhibits a (very small) decrease or increase in water vapor.**

***Index Terms*—Global Positioning System (GPS), radiosounding (RS), reprocessing, troposphere, water vapor.**

I. Introduction

OBSERVATIONS of atmospheric water vapor carried out in remote and inaccessible locations, such as the polar regions, are usually scarce and scattered, although crucial for defining the heat and radiation budget of the Earth's atmosphere. Due to the information they carry, their exploitation must be therefore pursued to a maximum extent.

Water vapor is the most abundant greenhouse gas and starts a positive radiative feedback mechanism of 1.5–2.0 $\mathrm{W \cdot m^{-2} \cdot K^{-1}}$, playing a central role in global warming [1]. It is essentially controlled by large-scale atmospheric dynamics and is mainly related to the moist air masses transported from the tropical upper troposphere toward higher latitudes. Water vapor creates a self-generating cycle, where its concentration and air temperature increase one another. Its relevant role is magnified by the interactions with the other greenhouse gases, carbon dioxide above all, whose effects are increased by anthropogenic factors, that may further amplify the water vapor feedback and drive future climate scenarios [2]. Water vapor concentrations, distribution, and variability within the planetary boundary layer and the free troposphere must be precisely determined to assess its heat trapping and the subsequent positive feedback processes affecting the Earth's climate. Quantification of the abundance and variability of atmospheric water vapor still requires longer and consistent time series of data, which are possibly recorded by different and independent sensors to overcome technique-specific systematic errors and to obtain accurate results.

Nowadays, spaceborne and ground-based observation techniques concur to the creation of data sets of water vapor, i.e., either layered or total (e.g., the National Aeronautics and Space Administration Water Vapor Project), that are stored and geared to user requirement specifications [3]. Although representing a few percentages of the total atmospheric content, Antarctic water vapor variations impact local temperature variations and play an important role in snowfall accumulation and surface mass balance [4]–[6]. Thus, accurate long time series of water vapor content in Antarctica are crucial to better understand the current climate variations and to assess the reliability of the predictions of global climate models. A decade of data or a longer time span is essential to detect reliable precipitable water vapor (PW) trends (cf. [7] and the references therein).

The propagation of the GPS radio signal through the atmosphere impacts the radio wave velocity according to the atmospheric media composition. In particular, the interaction with the unionized lower layers (stratosphere and troposphere) bends and delays the electromagnetic wave, introducing an error into the satellite slant range. Originally considered an observation nuisance, it is now more than two decades that the delay is used to reckon the atmospheric water vapor content and its variability [8]. The GPS-derived atmospheric water vapor has been used as an additional parameter in a number of tests and runs of mesoscale and synoptic-scale numerical weather prediction models and climate models [9]–[12].

In remote and hardly accessible areas, such as the vast majority of the Antarctic continent, unmanned observing systems are a compelling need. Thus, over the Antarctic coast, where the water vapor content is large enough to be detected by GPS, we selected a set of five GPS permanent stations whose data were used to compute the local integrated PW every 6 h with an accurate, reliable, and up-to-date estimation

Manuscript received January 20, 2015; revised June 13, 2015, October 22, 2015, and November 25, 2015; accepted December 9, 2015. This work was supported by Programma Nazionale di Ricerche in Antartide (PNRA) SCrl through the Mass Loss in Wind FluX (MALOX) Project under Grant PNRA-MIUR 2013/AZ3.03.

M. Negusini and P. Sarti are with the Institute of Radio Astronomy, Italian National Institute of Astrophysics, 40127 Bologna, Italy (e-mail: negusini@ira.inaf.it).

B. H. Petkov and C. Tomasi are with the Institute of Atmospheric Sciences and Climate, Italian National Research Council, 40129 Bologna, Italy.

Digital Object Identifier 10.1109/TGRS.2015.2509059

approach (see Section II). The fundamentals behind the GPS-based troposphere sensing are shortly illustrated in Section II, along with a description of the homogeneous reprocessing of the 12-year global GPS data set that we used to compute the PW content presented in this paper. The GPS results were validated using the radiosounding (RS) measurements collected over the same periods and locations; RS data were analyzed, minimizing and removing the known error sources and the instrumental biases (see Section III).

The sets of data that we used to compute the PW span the period from January 1, 1999 to December 31, 2010, with some scattered gaps over the time span, and they were collected at the following Antarctic stations (H is the height above the geoid).

1) Casey (CAS1; 66° 17′ S, 110° 32′ E; $H_{\rm RS} = 42$ m; $H_{\rm GPS} = 39$ m), with an overall number of 7652 PW estimates from Vaisala RS measurements and 15 624 from GPS.
2) Davis (DAV1; 68° 35′ S, 77° 58′ E; $H_{\rm RS} = 22$ m; $H_{\rm GPS} = 27$ m), with 7182 PW estimates from RS and 15 715 from GPS.
3) Mawson (MAW1; 67° 36′ S, 62° 52′ E; $H_{\rm RS} = 16$ m; $H_{\rm GPS} = 30$ m), where 6076 PW values were estimated from RS (once or twice per day, depending on the period), and 15 667 values were estimated from GPS observations.
4) McMurdo (MCM4; 77° 51′ S, 166° 40′ E; $H_{\rm RS} = 24$ m; $H_{\rm GPS} = 151$ m), with 5433 RS-derived PW estimates and 16 158 from GPS.
5) Mario Zucchelli (TNB1; 74° 42′ S, 164° 07′ E; $H_{\rm RS} = 55$ m; $H_{\rm GPS} = 127$ m), with an overall set of 1405 PW values derived from RS uniquely acquired during the Austral summer. These measurements were usually performed from October to February, but sometimes they were interrupted because of various instrumental defects. In particular, an unexpected interruption of the Vaisala Marwin Sounding System used to record pressure, temperature, humidity, and wind data caused a data loss from February 2004 until the end of 2005. At this site, the GPS time series also presents remarkable breaks, which are mainly due to power outages, i.e., from June 1999 to October 1999, the vast majority of 2008 and 2009, and from June to December 2010. The remaining data allowed us to estimate 11 870 PW values every 6 h.

Several studies compared the GPS performance in PW retrieval with other satellite, ground-based, and aerial methods, obtaining mostly an overall satisfying agreement in terms of relative variations but not always in terms of absolute values (e.g., see [13]). The biases are usually identified as systematic errors that are not properly handled in the data analysis of either technique. In order to overcome or, at least, minimize such biases, the use of proper models is crucial in the analysis of both GPS (see Section II-A) and RS data (see Section III-C).

II. Integrated PW From GPS

The GPS potential for the sensing of atmospheric water vapor was nicely illustrated in the early 1990s by Bevis *et al.* [8]. As the GPS signal travels through the troposphere, the total delay (TD, which is in meters) caused by the interaction with its constituents can be computed as [14]

$$\mathrm{TD} = \int_{\rm path} n(s)ds - \rho \tag{1}$$

where n is the air refractive index, and ρ is the slant range measured in meters. If the signal path bending is small, (1) can be evaluated along the geometric path as

$$\mathrm{TD} = \int (n(\rho) - 1)\, d\rho = 10^{-6} \int N(\rho) d\rho \tag{2}$$

with $N = 10^6(n-1)$, which is the refractivity of air; it can be expressed as $N = N_{\rm hyd} + N_{\rm wet}$, i.e., refractivity $N_{\rm hyd}$ due to atmospheric constituents without permanent dipole moment and $N_{\rm wet}$ due to water vapor (e.g., see [15]). Hence, (2) can be separated into two terms as follows:

$$\mathrm{TD} = 10^{-6} \left(\int N_{\rm hyd}(\rho) d\rho + \int N_{\rm wet}(\rho) d\rho \right). \tag{3}$$

The total delay depends on the (changing) satellite elevation above the horizon ε, i.e., TD(ε), and it is the sum of hydrostatic delay HD and wet delay WD (i.e., the delay due to water vapor) along the satellite antenna path (first and second addenda on the right-hand side of (3), respectively), i.e., $\mathrm{TD}(\varepsilon) = \mathrm{HD}(\varepsilon) + \mathrm{WD}(\varepsilon)$ [cf. (4)]. At every GPS site, it is convenient to express these quantities with respect to a univocal direction rather than the varying satellite elevation ε; hence, the local zenith direction ($\varepsilon = 90°$) is assumed as reference to express the zenith hydrostatic delay $\mathrm{HD}(90°) = \mathrm{ZHD}$ and the zenith wet delay $\mathrm{WD}(90°) = \mathrm{ZWD}$. The dimensionless mapping functions $m_{\rm hyd}(\varepsilon)$ and $m_{\rm wet}(\varepsilon)$ relate the total slant delay to the zenith delays as follows:

$$\mathrm{TD}(\varepsilon) = m_{\rm hyd}(\varepsilon) \cdot \mathrm{ZHD} + m_{\rm wet}(\varepsilon) \cdot \mathrm{ZWD}. \tag{4}$$

In GPS data analysis, the ZHD can be calculated *a priori* using a model [16], whereas the zenith total delay (ZTD) is estimated; as a result, the ZWD is obtained subtracting the *a priori* ZHD from the estimated ZTD as follows:

$$\mathrm{ZWD} = \mathrm{ZTD} - \mathrm{ZHD}. \tag{5}$$

The partial derivative used to relate the ZTD parameters to the observed phase, i.e., $\partial \mathrm{ZTD}/\partial\phi$, is usually the wet mapping function $m_{\rm wet}(\varepsilon)$ [17]. This means that the corrections to the ZHD, if required, are estimated as part of the corrections to the ZWD. Therefore, when aiming at determining accurate values of the ZWD (and PW), it is mandatory to compute the *a priori* ZHD with the utmost level of accuracy.

The PW (in millimeters) is finally obtained from the ZWD as [18]

$$\mathrm{PW} = \Pi \cdot \mathrm{ZWD}. \tag{6}$$

Dimensionless factor Π is given by

$$\Pi = \frac{10^6}{\rho R_w \left[(k_3/T_m) + k_2' \right]} \tag{7}$$

Fig. 1. Map showing the distribution of the GPS sites used in our study. The location of the five Antarctic stations for which the PW was computed is identified by black diamonds.

where ρ (in $\mathrm{kg \cdot m^{-3}}$) is the density of liquid water, and $R_w = 461.5\,\mathrm{J \cdot kg^{-1} \cdot K^{-1}}$ is the specific gas constant for water vapor. Parameters k_1, k_2, and k_3 ($k_2' = k_2 - mk_1$) have been introduced in the formula for refractivity in radio frequencies N [19], bearing in mind that $m = M_w/M_d$ is the ratio between the molar masses of water vapor and dry air. T_m (in kelvins) is a weighted mean temperature of the atmosphere, and according to the work in [8], it can be locally computed using RS measurements (see Section III-D).

A. GPS Data Processing

Space geodetic data spanning large time intervals require careful and homogeneous reprocessing to obtain consistent and unbiased estimates of long time series of geodetic parameters [20]–[23]. Some authors specifically addressed the reprocessing of GPS data aimed at computing TD (4) and PW (6) (see [24] and [25], respectively). Failures in the observable parametrization and modeling result in biased parameter estimates, as clearly shown in [26] precisely over the Antarctic continent.

The GPS solution was run in a double-differenced analysis approach over a modified version of the Bernese V.5.0 software [27]. Our modifications allowed us to introduce, select, and use the hydrostatic and wet Vienna Mapping Functions (VMF1) [28] and the Global Pressure and Temperature 2 (GPT2) model [29] to estimate the ZTD according to (4), which was assumed to give a more reliable estimate of the ZWD.

Along with our five Antarctic GPS stations (see Section I), we selected additional International Global Navigation Satellite System Service (IGS) permanent stations adopting the following criteria:

- having a homogeneous and global geographical distribution;
- having a long-term continuous observation history;
- having ITRF2008 coordinates and velocities [30];
- being designated as IGS08 core network stations (whenever possible).

A first run was performed to obtain consistent position time series of the GPS network (see Fig. 1); black diamonds identify the location of the five Antarctic stations where the PW was computed.

The 12-year data set was processed with the automatic processing tool Bernese Processing Engine. The analysis started from the observation files in the Receiver Independent Exchange (RINEX) format and aimed at producing and storing daily solutions in the Software Independent Exchange (SINEX) format and normal equations. A data sampling rate of 30 s and an elevation cutoff angle of 10° were used as the best compromise between the quantity and quality of data, this being a crucial aspect for high-latitude regions. The first-order term of the ionospheric refraction was eliminated by forming the ionosphere-free linear combination of the L1 and L2 signals. VMF1 hydrostatic and wet mapping functions were used for computing zenith delays TD. Corrections to *a priori* ZTD values were computed as piecewise linear functions with a time spacing of 1 h. The ambiguity resolution on all baselines was performed adopting the quasi-ionosphere-free strategy and the *a priori* global ionosphere models (GIMs) provided by the Center for Orbit Determination in Europe (CODE). The geodetic datum was defined by a no-net-translation condition with a tightly constrained approach, fixing a subset of ≈50 IGS stations that were considered those having the most reliable and stable *a priori* coordinates into ITRF2008. The most recent IGS08 products were adopted, and the complete list of parameters and models actually used in our analysis is shown in Table I. As aforementioned, this approach was used to compute a first solution where both coordinates and troposphere parameters were estimated.

A second run was performed (over the same set of GPS data) to estimate the ZTD. The models and parameters were not changed (see Table I), but we tightly constrained the coordinates of the whole network to the values obtained from the first run. This two-step procedure is also implemented by other authors (e.g., see [36] and [37]) and was adopted to

TABLE I
PARAMETERS AND MODELS USED IN THE GPS DATA ANALYSIS

Station coordinates / Sea surface heights	
Solid Earth tide	IERS Conventions, see [31]
Permanent tide	Conventional tide free system: IERS Conventions, see [31]
Ocean Tides	UTCSR Ocean Tide Model [32], [33] and Interpolation/Extrapolation [a]
Pole Tides	Linear trend for mean pole offsets: IERS Conventions, see [31]
Ocean Loading	FES2004 + TPXO.6.2 including the CoM correction for the motion of the Earth due to the ocean tides [b]
Atmospheric Loading	Not applied
Earth Orientation Parameters	
A priori information	IGS weekly ERP files (X-pole. Y-Pole, UT1-UTC) used with IGS precise orbits IG1[c]
Subdaily EOP Model	IERS2000
Nutation	IAU2000
Troposphere modeling	
Hydrostatic delay	Computed from 6-hourly ECMWF grids[d]
Mapping functions	VMF1, see [28]
Wet delay	Zero a priori model
Gradients	Zero a priori values, 24-h parameter estimated
Technique-specific models	
Phase center model	igs08_1685.atx [e], see [34]
Radome Calibrations	igs08_1685.atx
Antenna height	igs.snx + IGSSTATION [f]
Horizontal offsets	Applied
A priori radiation pressure	see [35]
A priori ionosphere models	CODE GIMs [g]

[a] ftp://ftp.csr.utexas.edu/pub/grav/OTIDES.CSRC

[b] http://holt.oso.chalmers.se/loading/

[c] ftp://cddis.gsfc.nasa.gov/gps/products/repro1

[d] http://ggosatm.hg.tuwien.ac.at/DELAY/

[e] ftp://igscb.jpl.nasa.gov/igscb/station/general/

[f] ftp://igscb.jpl.nasa.gov/igscb/station/log/

[g] ftp://ftp.unibe.ch/aiub/CODE/

decorrelate the positions (particularly the height component) from the troposphere estimates.

The computation of the ZHD to be used in (5) can be performed in different ways and is fundamental to obtain the propagation delay originated by the water vapor ZWD.

Here, we have computed the ZHD using the formula proposed in [8] and [38] as follows:

$$\mathrm{ZHD} = \frac{0.002277 \cdot p_s}{1 - 0.00266\cos(2\phi) - 0.00000028 \cdot h_s} \qquad (8)$$

that gives the ZHD in meters when the surface pressure at the site p_s is expressed in hectopascals, the ellipsoidal height of the site h_s is taken in meters, and latitude ϕ is in degrees. It is evident from (8) that, given the latitude and height of the GPS site, the surface pressure determines the values of the ZHD; it is worth recalling how a $+1$-hPa variation in (8) impacts the ZHD value by $\approx +2.2$ mm.

The pressure value at the GPS site p_s can be obtained in different ways. If automatic weather stations are located nearby the GPS site, p_s can be given by the local records of surface pressure and may be used in (8). Otherwise, the ZHD values at the latitude ϕ and longitude λ of the GPS site can be extracted from a grid $(2.5^\circ \times 2.0^\circ)$ provided by Technische Universität Wien (http://ggosatm.hg.tuwien.ac.at/DELAY/GRID, see Table I). The nodes of the grid are referred to as the ellipsoidal heights of an orographic surface. Values at any geographic location (ϕ, λ) can be obtained with a bilinear interpolation. The use of the grid is very convenient, as it does not require direct local pressure records that are seldom available in remote and isolated areas.

To obtain the $\mathrm{ZHD}_{\mathrm{grid}}$ value at the latitude ϕ and longitude λ of the GPS site, an interpolation from the nearest grid nodal points (i, j), $(i+1, j)$, $(i, j+1)$, and $(i+1, j+1)$ is required. A second transformation is necessary to account for the

height difference $\Delta h = h_{\rm grid} - h_s$ between the interpolated $\mathrm{ZHD}_{\rm grid}$ height and the actual GPS site height and to obtain the ZHD. In practice, $(\mathrm{ZHD}_{i,j}, \mathrm{ZHD}_{i,j+1}, \mathrm{ZHD}_{i+1,j}, \mathrm{ZHD}_{i+1,j+1}) \xrightarrow[\text{interpolation}]{\phi,\lambda} \mathrm{ZHD}_{\rm grid} \xrightarrow{\Delta h} \mathrm{ZHD}$.

In a previous study [39], we focused on the comparison of PW from GPS and RS data acquired at Mario Zucchelli and applied the method indicated in [40]. Once $\mathrm{ZHD}_{\rm grid}$ is computed, the corresponding pressure $p_{\rm grid}$ is obtained from (8); the height correction was achieved recalculating the ZHD with (8), where the new pressure is given by the pressure lapse rate formula proposed in [41], which defines p_s at the GPS site position (ϕ, λ, h_s) (in hectopascals) as

$$p_s = p_{\rm grid} + 1013.25(1 - 0.0000226 \cdot h_{\rm GPS})^{5.225} + - 1013.25(1 - 0.0000226 \cdot h_{\rm grid})^{5.225} \quad (9)$$

with pressure $p_{\rm grid}$ calculated in hectopascals at interpolated point $(\phi, \lambda, h_{\rm grid})$. Equation (9) does not contain the temperature, a variable on which the pressure lapse rate does indeed physically depend [42]. This can lead to errors in the ZHD varying between 10 and 25 mm, as confirmed by our work carried out to analyze the data set collected at the Mario Zucchelli station [39].

There, we used: 1) $\mathrm{ZHD}_{\rm grid}$, (8), and (9) to account for height difference Δh and to obtain the ZHD; and 2) the local records of surface pressure p_s to derive the ZHD from (8). The former method showed a large wet and seasonal bias of $\mathrm{PW}_{\rm GPS}^{\rm grid}$ (the subscript and the superscript identify the calculation method). In particular, assuming the time series of precipitable water $\mathrm{PW}_{\rm TOT}$ (determined as the sum of the tropospheric contribution derived from RS data and the stratospheric contribution derived from satellite data, as explained in detail in Section III-C) as the benchmark, $\mathrm{PW}_{\rm GPS}^{\rm grid}$ was 55% larger than $\mathrm{PW}_{\rm TOT}$, thus highlighting a remarkable wet bias in the GPS results. The GPS-derived values directly obtained from (8) inserting the local records of p_s, i.e., $\mathrm{PW}_{\rm GPS}^{p_s}$, were determined as being only 77% of $\mathrm{PW}_{\rm TOT}$, with a better overall agreement but a dry bias. We related the worse performance of $\mathrm{ZHD}_{\rm grid}$ to pressure correction Δh [calculated with (9)]. For the Mario Zucchelli station, we had to accommodate a very large height difference, being $\Delta h \approx 1000$ m. Similar features can be found in other Antarctic coastal areas where massive mountain ranges are close to the sea, as explicitly discussed in [29]. There, the ellipsoidal heights of four adjacent nodes of the grid may considerably vary, and the interpolation may lead to a $\mathrm{ZHD}_{\rm grid}$ whose height is considerably different from the actual GPS height. Under these circumstances, height correction $\mathrm{ZHD}_{\rm grid} \xrightarrow{\Delta h} \mathrm{ZHD}$ becomes critical, and (9) is not accurate enough, as was also highlighted in [43].

In this paper, we transformed $\mathrm{ZHD}_{\rm grid} \xrightarrow{\Delta h} \mathrm{ZHD}$ with the formula proposed in [43] as follows:

$$\mathrm{ZHD} = \mathrm{ZHD}_{\rm grid} + 0.0022768 \cdot \left(\frac{g \cdot p_{\rm grid}}{R \cdot T_{\rm grid}}\right) \cdot (\Delta h) \quad (10)$$

where $g = 9.8\ \mathrm{m \cdot s^{-2}}$ is the gravity acceleration, and $R = 8.314\ \mathrm{J \cdot K^{-1} \cdot mol^{-1}}$ is the gas constant. The temperature and pressure at the interpolation point, i.e., $T_{\rm grid}$ and $p_{\rm grid}$, respectively, have been extracted from the new GPT2 model that ensures good performance over the Antarctic coast [29]. The ZHD at the GPS site was obtained from $\mathrm{ZHD}_{\rm grid}$ using correction formula (10), and (5)–(7) allowed us to compute the $\mathrm{PW}_{\rm GPS}$ time series at 00:00, 06:00, 12:00, and 18:00 Coordinated Universal Time (UTC), where each value yields the precipitable water averaged over the hh:mm–hh:mm+1 h time interval. These time series were subsequently compared with those derived from the RS data, as described in Section III (see Fig. 2).

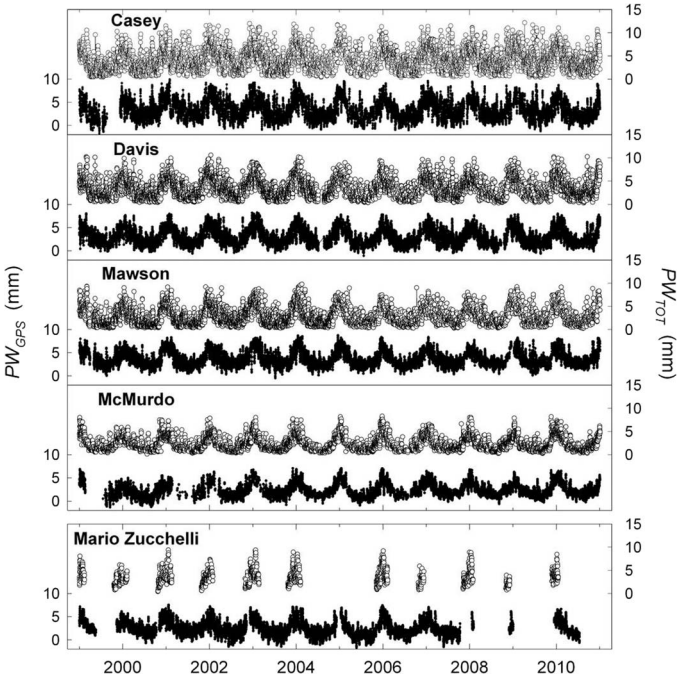

Fig. 2. PW time series from GPS observations [$(\mathrm{PW}_{\rm GPS})$, as shown by solid black circles in the scale on the left in millimeters] and RS data [$(\mathrm{PW}_{\rm TOT})$, as shown by open black circles in the scale on the right in millimeters]. See Section III for the computational details for the five Antarctic sites.

Mean temperature T_m in (7) was calculated using the RS data according to the following, as described in Section III-D:

$$T_m = \frac{\int_{z_0}^{z_{\rm TR}} (e(z)/T(z))\, dz}{\int_{z_0}^{z_{\rm TR}} (e(z)/T(z)^2)\, dz}. \quad (11)$$

III. RS Measurements

The Casey, Davis, and Mawson RS stations in Antarctica are managed by the Bureau of Meteorology, and the Vaisala radiosonde data sets recorded at these three stations were downloaded from the World Meteorological Organization (WMO) database of the University of Wyoming (http://weather.uwyo.edu/upperair/sounding.html). They consist of an overall number of 20 910 RSs conducted over the 12-year period. The set of radiosonde data collected at the McMurdo station by the U.S. National Weather Service was downloaded from the aforementioned WMO database, obtaining an overall number of 5433 RSs over the 12-year period. The RS data recorded at the Mario Zucchelli station were collected by the

Meteo-Climatological Observatory (http://www.climantartide.it) from January 1999 to early February 2004 and from November 2005 to December 2009 because of the aforementioned instrumental failures. Therefore, an overall number of 1405 RSs were collected at this coastal station for the present analysis.

A. Correction of Raw Pressure and Temperature Measurements

An overall set of 27 748 Vaisala RSs were collected at the aforementioned selected five coastal Antarctic stations over the 12-year period, examining the measurements provided at numerous levels by the Barocap, Thermocap, and Humicap sensors mounted on the various radiosonde models. At all the five sites, RS launches were regularly performed at 00:00 and 12:00 UTC of each day. On the Austral summer days, each RS provided measurements of pressure $p(z)$ and air temperature $T(z)$ at more than 800 standard and additional altitudes z from surface to 10 km and 900–1900 stratospheric levels up to its top altitude, usually ranging from 26 to 30 km. Due to the harder environmental conditions, the RS data were collected on Austral spring and fall days at no more than 800 levels from surface to 10 km and no more than 200–400 stratospheric levels up to a radiosonde top level varying from 18 to 25 km. Relative humidity RH(z) was usually measured at about 800 tropospheric levels and only a few levels above the tropopause because RH(z) is usually lower than a few percent at levels $z > 8$ km.

The measurements of $p(z)$ (given in hectopascals), $T(z)$ (in degrees Celsius), and RH(z) (in percentage) were recorded in height steps of 10–12 m for the mean balloon ascent rate of 5–6 m $\cdot$ s^{-1}. Altitude z was calculated for each triplet of RS signals using the manufacturer algorithm based on the differential form of the hydrostatic equilibrium equation for air. No corrections were made to the raw pressure data provided by the radiosondes since the instrumental errors were assumed to be < 0.5 hPa in all cases for the Barocap characteristics reported in Table II.

The temperature data provided by the various Thermocap sensors are usually affected by errors due to: 1) heating by the incoming solar radiation and cooling induced by the outgoing flux of infrared radiation; 2) heat conduction from the other radiosonde components; and 3) heat exchanges between the sensor and environment, leading to the evaluations of accuracy, repeatability, and reproducibility characteristics given in Table II. The errors affecting the RS80-A and RS80-H Thermocap sensors were corrected according to the work in [44], whereas those of the RS90 and RS92 Thermocap sensors were neglected [45]. The RS80 and RS90/92 Thermocap data are also often affected by lag errors mainly depending on air density and ventilation speed, which were corrected by using the algorithm in [46] over the whole altitude range above the ground layer. According to the work in [47], null errors were assumed for isothermal conditions of the ground layer, and linearly increasing errors were assumed for increasing positive values of the vertical temperature gradient $\gamma = dT/dz$ until reaching an RS80 value of 1.0 K for $\gamma \geq 1$ K/m and an average RS90/92 value of 1.2 K for $\gamma \geq 1.4$ K/m [48].

B. Corrections of Raw RH Measurements

The time constant of the A-Humicap sensor was estimated to increase in a nearly exponential fashion from 0.2 to about 200 s as $T(z)$ decreases from 25 °C to −80 °C, with a mean vertical gradient of 6–7 K/km [48]. Conversely, the H-Humicap time constant was evaluated to be very small, which is due to the use of a thinner polymer layer in this sensor model, assuring a much faster response time at low temperatures [49]. The RH data provided by the H-Humicap sensors were therefore corrected by taking into account the improved time constant characteristics of these sensors, which were determined by following a complex procedure based on the combined use of various algorithms and correction procedures [48], [50] and adopting some important criteria recommended in various articles [49], [51], [52]. More precisely, the original RH data were analyzed through a procedure consisting of the following seven steps.

1) A preliminary smoothing procedure of the raw RH data within all the height intervals containing sequences of constant values of RH with altitude to construct a more schematic "skeleton" of the vertical profiles of RH [48].
2) A correction of the RH data for the so-called basic calibration model errors using the algorithms defined in [50] for the RS80-A and RS80-H Humicap sensor models and those defined in [49] and [52] for the RS90 and RS92 Humicap sensor models.
3) The correction of the chemical contamination (CC) dry biases affecting the RH data recorded with the four RS80-A, RS80-H, RS90, and RS92 radiosonde models was made by assuming that: 1) the CC biases affecting the RS80 data are all negligible in sensors having an age of a few years; 2) those of the RS90 sensors are totally negligible since polymers with improved characteristics were employed in manufacturing this new sensor model [48]; and 3) those of the RS92 sensors were assumed to be very small since such sensors were all properly heated and regenerated prior to their launch.
4) The correction of temperature-dependent dry biases was made by: 1) using the algorithms defined in [50] to examine the RS80-A and RS80-H data according to [53]; and 2) totally neglecting the temperature-dependent errors affecting the RS90 and RS92 sensors [49].
5) The correction of the RH data for the sensor aging (SA) dry biases was made by using the algorithm in [50] to remove the errors of the RS80-A and RS80-H Humicap sensors, which were evaluated to not exceed 2% in all cases. The SA dry biases of the RS90 and RS92 Humicap sensors were all neglected according to the work in [49].
6) A correction of all the RH vertical profiles obtained at step 5 was made to remove the RH lag errors by following the procedure in [48] consisting of: 1) a first smoothing procedure; 2) a lag correction procedure properly adapted to the various RS80-A, RS80-H, RS90, and RS92 Humicap sensors by the work in [48]; and 3) a further smoothing procedure, reducing even more the discontinuities appearing in the RH vertical profiles.

TABLE II
CHARACTERISTICS, WHICH ARE GIVEN BY THE MANUFACTURER OR DRAWN FROM THE LITERATURE, OF THE BAROCAP, THERMOCAP, AND HUMICAP SENSORS MOUNTED ON THE FOUR VAISALA RADIOSONDE MODELS AT THE FIVE ANTARCTIC SITES CONSIDERED IN THIS PAPER

Characteristics	Vaisala Radiosonde Model			
	RS80-A	**RS80-H**	**RS90**	**RS92**
BAROCAP SENSOR (values in hPa)				
Measurement range	$1060-3$	$1060-3$	$1080-3$	$1080-3$
Declared resolution	0.1	0.1	0.1	0.1
Accuracy	± 0.5	± 0.5	± 0.5	± 0.5
Repeatability in calibration [range]	0.5	0.5	0.4 [1080 − 100] 0.3 [100 − 3]	0.4 [1080 − 100] 0.3 [100 − 3]
Reproducibility in sounding [range]	0.5	0.5	0.5 [1080 − 100] 0.3 [100 − 3]	0.5 [1080 − 100] 0.3 [100 − 3]
THERMOCAP SENSOR (values in K)				
Measurement range	$333-183$	$333-183$	$333-183$	$333-183$
Declared resolution	0.1	0.1	0.1	0.1
Accuracy	± 0.2	± 0.5	± 0.5	± 0.5
Repeatability in calibration	0.2	0.2	0.15	0.15
Reproducibility in sounding [range (in hPa)]	0.2 [1060 − 50] 0.3 [50 − 15] 0.4 [15 − 3]	0.2 [1060 − 50] 0.3 [50 − 15] 0.4 [15 − 3]	0.2 [1080 − 100] 0.3 [100 − 20] 0.5 [20 − 3]	0.2 [1080 − 100] 0.3 [100 − 20] 0.5 [20 − 3]
HUMICAP SENSOR (values in % RH)				
Measurement range	$2-100$	$0-100$	$0-100$	$0-100$
Declared resolution	1	1	1	1
Accuracy	$< \pm 3$	± 5	± 5	± 5
Repeatability in calibration	2	2	2	2
Reproducibility in sounding	< 3	< 3	< 3	2

7) A correction of all the dry biases affecting the RS92 RH data was made on the basis of the comparison tests performed in [52] between the RS92 RH data and those provided by some reference sensors for minimizing the daytime solar radiation error (SRE) and other empirical solar heating (SH) dry biases using the original algorithm of the work in [54] adapted to the Antarctic atmosphere conditions [53]. Instrumental errors and empirical biases such as those shown in [52] were neglected in analyzing the RS80 Humicap data, and the SH dry biases of the RS90 and RS92 Humicap sensors were not corrected in the present analysis since they were already accounted for using the correction procedure in [52], in which the similar errors of the RS90 and RS92 Humicap sensors were already taken into account, whereas the empirical mean SH dry biases and SREs affecting the RS90 and RS92 radiosonde data were corrected using the pair of algorithms defined in [52].

C. Calculations of Precipitable Water From RS Data

The values of $p(z)$, $T(z)$, and $\mathrm{RH}(z)$ determined at each level z using the aforementioned correction procedures were then examined to calculate the following: 1) saturation water vapor pressure $E(T)$ in the pure phase over a plane surface of pure liquid water using the Murphy and Koop [55] formula (see also [56]), as determined on the basis of some recent measurements of molar heat capacity over the 123–332 K temperature range; 2) water vapor partial pressure $e(z)$ given by product $E[T(z)] \cdot \mathrm{RH}(z)$; and 3) the water vapor mixing ratio given by ratio $e(z)/p(z)$. Therefore, the aforementioned formulas were reliably used for the very-low-temperature conditions observed in the Antarctic troposphere and low stratosphere, obtaining realistic evaluations of $E[T(z)]$ to determine the absolute humidity $q(z)$ at each level in terms of the ratio between $e(z) = E[T(z)] \cdot \mathrm{RH}(z)$ and product $T(z) \cdot R_w$. These calculations of $E[T(z)]$ derived at the various levels using the Murphy and Koop formula over the 190–280 K temperature range were found to be fully reliable since they differ from: 1) those given by the Goff and Gratch formula [57] over the 223–290 K temperature range by percentages varying from $+0.15\%$ at 275 K to less than $+0.1\%$ at 230 K; and 2) those of the Bolton [58] formula over the 238–290 K temperature range by percentages varying from -0.2% at 240 K to $+0.1\%$ at 285 K. The aforementioned evaluations of $q(z)$ found for each RS were used to determine the vertical profile of such a parameter by assuming

that it varies in an exponential fashion as altitude z increases from one radiosonde level to the next. The atmospheric PW_{RS} was determined by integrating $q(z)$ from the surface level up to the 12-km height. These evaluations of PW_{RS} seem to be fully reliable since they were obtained for the vertical profiles of $T(z)$ and $RH(z)$ appropriately corrected for the main lag and instrumental errors and the various dry biases. The values of water vapor mixing ratio $e(z)/p(z)$ mainly ranged from 2 to 7 parts per million by volume at the upper tropospheric levels [59] and the stratospheric levels [3]. Therefore, the stratospheric PW_{ST} content above the 12-km altitude turns out to be very low in the Antarctic atmosphere, mainly varying from $3 \cdot 10^{-3}$ to $6 \cdot 10^{-3}$ mm throughout the year at the 65° S–80° S latitudes. However, we have corrected the values of tropospheric precipitable water PW_{RS} determined up to the 12-km altitude by adding the monthly average values of stratospheric PW_{ST} derived from the observations carried out using the Michaelson Interferometer for Passive Atmospheric Sounding (MIPAS)–Environmental Satellite (ENVISAT) [60] to obtain the total precipitable water $PW_{TOT} = PW_{RS} + PW_{ST}$. The comparison between RS RH measurements and those carried out by a reference instrument [49], with accuracy performance varying from 3% to 6% in the troposphere, showed that, after the corrections given in Section III-B, the RS data became closer to the standard, presenting discrepancies of 1%–3% only. Bearing in mind that the temperature is registered by the radiosonde with an error lower than 1% and that the main contribution to the water vapor content is given by the troposphere, the error made in estimating PW_{TOT} results in no higher than 10%. The time series of the daily values of total precipitable water PW_{TOT} are shown in Fig. 2 for the five RS sites. It can be seen that PW_{TOT} is subject at all sites to marked day-to-day variations, presenting month-to-month and seasonal variations describing a wide minimum during the coldest (Austral winter) months of the year, i.e., from April to September. The results show that marked variations in PW_{TOT} may occur within a few days, which is due to sharp variations in the meteorological conditions caused by the arrival of more humid and warmer air masses from the oceans or associated with drier and colder air masses driven by katabatic winds toward the coasts. In particular, lower values of PW_{TOT} were found at McMurdo during the Austral winter than at Casey, Davis, and Mawson presumably because of its higher latitude and colder temperature conditions, whereas values comparable with those measured at Mario Zucchelli were determined during the Austral summer. The analysis of RS data showed that the minima of PW_{TOT} recorded at Casey, Davis, Mawson, and McMurdo were, in general, all lower than 1 mm during the coldest period of the Austral winter, and the maxima exceeded 12 mm at Casey, 10 mm at Davis and Mawson, and 8 mm at McMurdo during the Austral summer; on the other hand, the daily values of PW_{TOT} determined at Mario Zucchelli mainly ranged from 2 to 8 mm over the October–February period and were, in general, lower than 10 mm on the warmer summer days. The comparison made in Fig. 2 between the time series of PW_{GPS} and those of PW_{TOT} derived from the RS and MIPAS data clearly shows that a substantial agreement exists at all the five Antarctic sites.

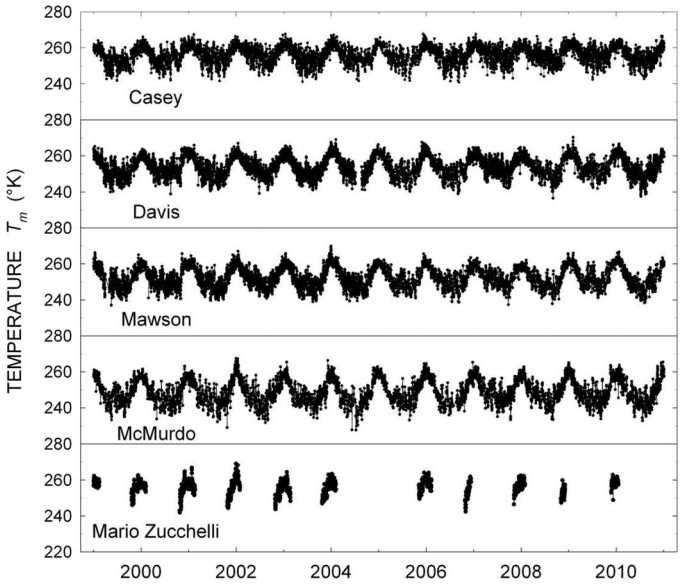

Fig. 3. Time series of parameter T_m obtained from the RS measurements conducted during the 12-year period at the five Antarctic stations.

D. Calculations of the Weighted Mean Temperature T_m

Parameter T_m is the average value of air temperature weighted along the vertical atmospheric path by using the vertical profile of $e(z)$ as a weight function. It is calculated using the algorithm of (11) [16] given by the ratio between the two integrals determined over the altitude range from surface level z_0 to $z_{TR} = 12$ km, where the vertical profiles of $e(z)$ and $T(z)$ were derived from the RS measurements recorded on each day at one of the five sites considered in this paper and examined using the seven-step correction procedure described earlier. Considering that parameter $e(z)$ is used in (11) as a weight function in both integrals, parameter T_m can be defined in practice as the average tropospheric temperature calculated as the sum of the contributions given by the various atmospheric layers weighted on the basis of their moisture characteristics.

The time series of the daily mean values of T_m obtained at the five Antarctic stations over the 12-year time span are shown in Fig. 3. The results provide evidence of the marked seasonal variations in T_m, which is most strongly influenced by the thermal characteristics of the Antarctic atmosphere in its most humid layers. It can be seen in Fig. 3 that T_m appreciably varies from one day to another at Casey, Davis, and Mawson, showing average annual time patterns describing very similar seasonal cycles. The McMurdo and Mario Zucchelli stations are ≈ 300 km far one from the other, being located at longitudes and latitudes differing by 2° 33′ and more than 3°, respectively. Marked day-to-day variations in T_m can be noted in all years. As shown in the lowest panels in Fig. 3, the average seasonal variations are similar from one year to another, only presenting slight discrepancies in the Austral summer months.

Examining the Mario Zucchelli set of 1330 RSs in [46], it was shown that the vertical profile of $T(z)$ exhibits a stable vertical gradient from z_0 to tropopause level z_{TR} (which is close to 8 km during the Austral summer). Calculations of $T_m(z)$ were made in terms of (11), where the numerator and denominator

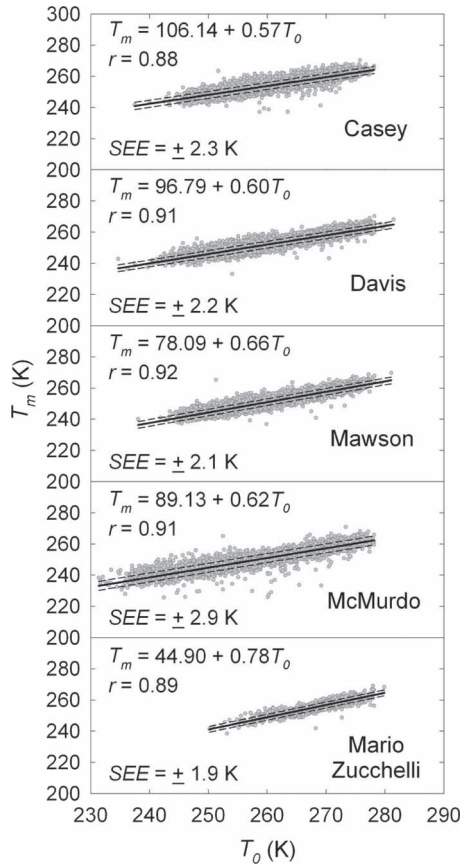

Fig. 4. Scatter plots of parameter T_m versus ground-level temperature T_0 obtained by examining the RS data sets over the 12-year period, with the corresponding equations of the best fit lines, the values of correlation coefficient r, and the SEE.

integrals were evaluated for the RS data sets collected at Mario Zucchelli on Austral summer days and McMurdo on Austral winter days, finding that $T_m(z)$ gradually increases as a function of z until reaching an asymptotic value at altitudes $z > 8$ km. In addition, these calculations indicate that ground-level temperature T_0 is a thermal parameter yielding realistic information of the thermal state of the whole troposphere and therefore can be reliably used to represent the average thermal conditions of the troposphere throughout the entire year. This can be seen in Fig. 4, in which the values of T_m calculated at each station in terms of (11) are plotted versus those of T_0. The scatter plots obtained for the Casey, Davis, and Mawson data sets were found to yield regression lines of T_m versus T_0, with values of correlation coefficient r ranging from 0.88 to 0.92; hence, it is comparable with the value of $r = 0.91$ obtained at McMurdo over the whole year and with $r = 0.89$ determined at Mario Zucchelli over the Austral summer only. A good agreement was also found among the values of slope coefficient k determined at the five stations, and they were found to vary between $+0.57$ K^{-1} (at Casey) and $+0.66$ K^{-1} (at Mawson) over the whole year and to be equal to $+0.78$ K^{-1} at Mario Zucchelli for the Austral summer only. Therefore, the scatter plots shown in Fig. 4 exhibit a very good correlation between T_m and T_0, with the respective standard errors of the estimate (SEEs) found to range from ± 1.9 (Mario Zucchelli) to ± 2.9 K (McMurdo). A similar relationship between T_m and T_0 was reported in [18], where it was concluded that the approximation uncertainties led to about 2% error in T_m.

It is worth highlighting that, due to the lack of year-round RS measurements at Mario Zucchelli (causing a lack of T_m), the $T_m - T_0$ relation in Fig. 4 was actually implemented to calculate the $\mathrm{PW_{GPS}}$ values given in Fig. 2 using the surface temperature acquired at the automatic weather station Eneide, which is similar to the work in [39].

IV. Comparison Between GPS and RS Evaluations of Precipitable Water

The $\mathrm{PW_{TOT}}$ time series were used as a benchmark to assess the quality of the GPS results. As described in Section III, the RS sensors at all sites are of the same type and manufacturer and required the same corrections to account for and mitigate their known biases. Thus, the RS $\mathrm{PW_{TOT}}$ time series at every site can be certainly regarded as consistent and useful to evaluate the reliability of the corresponding GPS time series of $\mathrm{PW_{GPS}}$. The comparison of $\mathrm{PW_{GPS}}$ with the results provided by the colocated RS observations can be considered an approach to approximately assess the error in the precipitable water determined by the GPS technique at the selected sites [25].

The 12-year time series values of PW derived from the GPS and RS data at the five Antarctic sites are plotted in Fig. 2. A rather good qualitative agreement between the time series is clearly visible, with evident and consistent time patterns and reasonable seasonal features; at all sites, small PW values correspond to the (dryer) winters, whereas larger values of PW are detected during the (more humid) Austral summers. In the GPS time series (solid black circles), very few negative values of $\mathrm{PW_{GPS}}$ occur and are visible in the plots of the various sites during the winter periods. This happens when ZHD from (8) and used in (5) is larger than the estimated ZTD, thus causing ZWD (and $\mathrm{PW_{GPS}}$) to be negative. An estimate of the accuracy of $\mathrm{PW_{GPS}}$ can be obtained with the formula given in [61] as follows:

$$\sigma_{\mathrm{PW}}^{\mathrm{GPS}} = \sqrt{\left(\frac{\mathrm{ZWD}}{a}\cdot\sigma_{T_m}\right)^2 + (\Pi\cdot b\sigma_p)^2 + (\Pi\cdot\sigma_{\mathrm{ZTD}})^2} \tag{12}$$

where $a = 1768.72$ K, and $b = 0.00228$ m $\cdot$ hPa^{-1}. In particular, using a 2% error for T_m (see Section III-D), a 2-hPa error for the European Center for Medium-Range Weather Forecasting (ECMWF) pressure (used to compute $\mathrm{ZHD_{grid}}$) given by the work in [40], and the errors for ZTD from our GPS analysis (0.6–1 mm), an average error of $\sigma_{\mathrm{PW}}^{\mathrm{GPS}} \approx 0.7$ mm was found. In [61], from a comparison between GPS and Very Long Baseline Interferometry data, a more realistic 4–10-mm ZTD error is calculated. Therefore, assuming 10-mm accuracy for ZTD, from (12), we get a $\sigma_{\mathrm{PW}}^{\mathrm{GPS}} \approx 1.6$ mm. This estimate is consistent with the accuracy given in [61] and the references therein and accounts for all the (very few) negative values found in the $\mathrm{PW_{GPS}}$ time series (see Fig. 2).

In order to quantify the extent of the agreement and identify possible biases, the scatter plots and the correlation coefficient

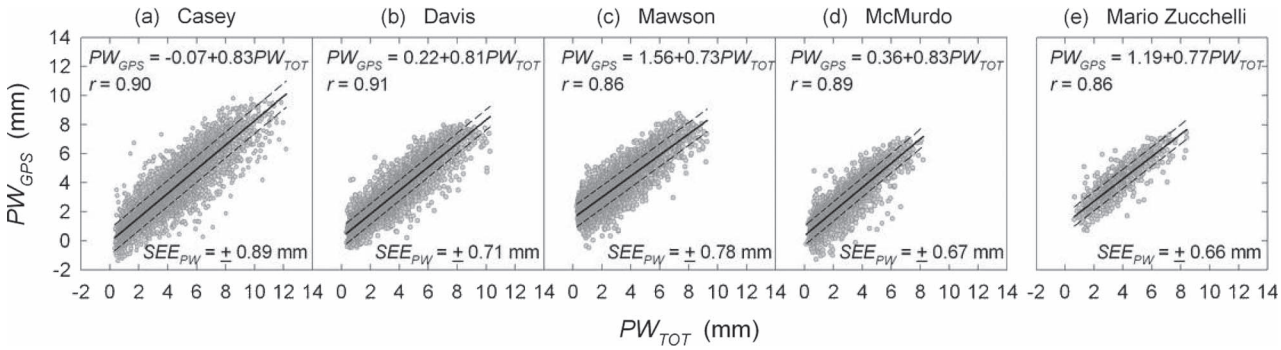

Fig. 5. Scatter plots of $\mathrm{PW_{GPS}}$ versus $\mathrm{PW_{TOT}}$. The values of $\mathrm{PW_{GPS}}$ were obtained using the T_m values computed in Section III-D. Concerning Mario Zucchelli, $\mathrm{PW_{GPS}}$ was obtained though the $T_m - T_0$ relation using the surface temperature acquired at the weather station Eneide. The equations of the best fit lines, the values of correlation coefficient r_{PW}, and $\mathrm{SEE_{PW}}$ are given in each of the panels.

TABLE III
VALUE OF PARAMETERS CHOSEN TO COMPARE GPS AND RS TECHNIQUES. IN THE FIRST TWO LINES, THE PW MEAN VALUES FOR BOTH GPS AND RS ARE PRESENTED. IN THE THIRD LINE, THE MEAN VALUE OF THE RATIO Ψ [SEE (13)] BETWEEN THE TWO PW VALUES IS REPORTED. THE VALUES IN BRACKETS GIVEN IN THESE THREE LINES ARE THE CORRESPONDING STANDARD ERROR OF THE ESTIMATES. IN THE FOLLOWING EIGHT LINES, THE LINEAR TRENDS α, AMPLITUDES A, PERIODS T, AND PHASES φ OF THE PERIODIC SIGNAL, WHICH ARE PRESENT IN BOTH TIME SERIES, ARE SHOWN. THE LAST LINE REPORTS THE HEIGHT DIFFERENCE $\Delta H = H_{\mathrm{GPS}} - H_{\mathrm{RS}}$ BETWEEN THE GPS AND RS SITES. THE LARGE ΔH AT THE MCMURDO AND MARIO ZUCCHELLI STATIONS ARE ACCOUNTED FOR IN THE LAST TWO COLUMNS, WHERE $\mathrm{PW_{TOT}}$ IS COMPUTED ONLY USING THE DATA ACQUIRED FROM THE GPS SITE HEIGHT ONWARD

Parameter	Casey	Davis	Mawson	McMurdo	Mario Zucchelli	*McMurdo*$^{(127)}$	*Mario Zucchelli*$^{(72)}$
$\overline{PW_{GPS}}$ (mm)	3.43 (0.01)	3.02 (0.01)	3.68 (0.01)	2.29 (0.01)	2.46 (0.01)	—	—
$\overline{PW_{TOT}}$ (mm)	4.18 (0.02)	3.50 (0.02)	2.95 (0.02)	2.42 (0.01)	3.57*(0.04)	*2.31 (0.01)*	*3.57*(0.04)*
Ψ	0.80 (0.01)	0.91 (0.01)	1.63 (0.13)	1.03 (0.01)	1.15 (0.01)	*1.08 (0.01)*	*1.16 (0.01)*
α_{GPS} (mm/yr)	-0.03 ± 0.01	0.00 ± 0.01	-0.01 ± 0.01	0.01 ± 0.01	—	—	—
α_{TOT} (mm/yr)	0.04 ± 0.01	0.00 ± 0.01	0.01 ± 0.01	0.00 ± 0.01	—	*0.00 ± 0.01*	—
A_{GPS} (mm)	1.74 ± 0.03	1.74 ± 0.02	1.56 ± 0.02	1.44 ± 0.02	—	—	—
A_{TOT} (mm)	1.60 ± 0.03	1.79 ± 0.02	1.76 ± 0.02	1.50 ± 0.02	—	*1.41 ± 0.02*	—
T_{GPS} (days)	366.4 ± 0.2	364.7 ± 0.2	364.5 ± 0.2	366.3 ± 0.2	—	—	—
T_{TOT} (days)	366.7 ± 0.3	365.0 ± 0.2	364.7 ± 0.2	366.2 ± 0.2	—	*366.2 ± 0.2*	—
φ_{GPS} (rad)	1.39 ± 0.03	1.18 ± 0.02	1.18 ± 0.02	1.48 ± 0.02	—	—	—
φ_{TOT} (rad)	1.38 ± 0.04	1.20 ± 0.03	1.19 ± 0.03	1.47 ± 0.02	—	*1.46 ± 0.02*	—
ΔH (m)	-3	5	14	127	72	//	//

* Computed with Austral summer data only, see Fig. 2.

are extremely effective. Such a comparison was made by plotting the measurements of $\mathrm{PW_{GPS}}$ versus those correspondingly obtained for $\mathrm{PW_{TOT}}$. As aforementioned, the latter parameter was derived from RS measurements conducted at 00:00 and 12:00 UTC of each day by adding the stratospheric content. In order to carry out a more homogeneous comparison test that is an important issue [62], only the values of $\mathrm{PW_{GPS}}$ obtained at the two aforementioned UTC hours were selected for the comparison. Fig. 5 depicts the linear regression scatter plots drawn for the PW data set at each site, separately presenting the values of $\mathrm{PW_{GPS}}$ as a function of $\mathrm{PW_{TOT}}$ at each station. The values of correlation coefficient r were found to vary from $r = 0.86$ at Mawson and Mario Zucchelli to $r = 0.91$ at Davis. A similar comparison between GPS and RS techniques, which was performed by analyzing the PW data sets for 2004 at various Antarctic sites, including Casey, Davis, Mawson, and McMurdo, was reported in [26]. Thomas *et al.* [26] calculated higher slope coefficients than those given in Fig. 5 that can be accounted for the appreciably shorter period used in their study, which excluded the impact of the interannual PW variability. In fact, the scatter plots constructed only for the 2004 data, which were extracted from the analyzed data sets here (cases not shown in Fig. 5), highlighted slope coefficients that were consistent with those found in [26].

Mean values $\overline{\mathrm{PW_{GPS}}}$ and $\overline{\mathrm{PW_{TOT}}}$, which were computed for the corresponding PW values over the analyzed period, are reported in the first two lines in Table III. The GPS technique detects the smaller mean content of PW at McMurdo and Mario Zucchelli, whereas the other three sites appear to be more humid on average, particularly at Mawson and Casey. A similar conclusion can be drawn from the results of the RS observations: The Australian sites are more humid than McMurdo. Most probably, this also holds for Mario Zucchelli, but no definite statements can be made since $\overline{\mathrm{PW_{TOT}}} = 3.57$ mm

only corresponds to Austral summer observations. The largest discrepancies between the two techniques is $\approx$ 0.75 mm found at Mawson and Casey, although with different signs: At Mawson station, $\overline{\mathrm{PW_{GPS}}} > \overline{\mathrm{PW_{TOT}}}$, whereas it is the opposite for Casey.

An additional indicator of the consistency of the results is represented by the mean value of the $\mathrm{PW_{GPS}}/\mathrm{PW_{TOT}}$ ratio, which is defined as

$$\Psi = \overline{\left(\frac{\mathrm{PW_{GPS}}}{\mathrm{PW_{TOT}}}\right)} \tag{13}$$

which is also very useful to spotlight the presence and extent of biases between the time series. The third line in Table III reports the values of Ψ, which were computed for nearly simultaneous data available for the selected stations. It is seen that ratio Ψ does not define a clear and consistent situation in terms of the biases between the two techniques. At Davis and Casey, where the height difference between the RS launch and GPS sites does not exceed a few meters (i.e., the observations start and interact with the same atmospheric layers, the lowest line in Table III), the $\mathrm{PW_{GPS}}$ time series exhibit a dry bias with respect to $\mathrm{PW_{TOT}}$, leading to a ratio < 1. At Mawson, where $\Delta H = 14$ m is also rather small, $\mathrm{PW_{GPS}}$ is 63% larger than $\mathrm{PW_{TOT}}$, and the corresponding time series overestimates the water vapor content by a remarkable amount. This large wet bias is also associated to larger scatter of the PW values, making Mawson's results the least accurate and satisfactory among all. At both McMurdo and Mario Zucchelli stations, the GPS site is located several tens of meters above the RS launch site. A dry bias in $\mathrm{PW_{GPS}}$ may be actually expected as a consequence of the thinner portion of atmosphere actually traveled by the GPS signal. Nevertheless, this is clearly not the case, as the ratio highlights a wet bias for $\mathrm{PW_{GPS}}$ at Mario Zucchelli by about 15% of the corresponding $\mathrm{PW_{TOT}}$. Finally, the best agreement above all is detected at McMurdo ($\Psi = 1.03 \pm 0.01$), where, due to the largest height difference ΔH, the largest GPS dry bias could be also expected. In order to account for the different ΔH at these two sites, $\mathrm{PW_{TOT}}$ were locally recomputed, discarding the observations acquired below the GPS site heights. As expected, the new $\mathrm{PW_{TOT}}$ for McMurdo and Mario Zucchelli are smaller, with a further increase in the wet GPS bias of 5% and 1% for the two stations, respectively (last two values in the third line in Table III). It is worth noting that biases are also due to the different measurement time periods of $\mathrm{PW_{GPS}}$ and $\mathrm{PW_{TOT}}$. In fact, the $\mathrm{PW_{GPS}}$ calculation time is equal to 1 h, whereas that of $\mathrm{PW_{TOT}}$ requires approximately 35 min for the whole RS monitoring of the tropospheric thermodynamic conditions from the surface to a 12-km altitude.

To examine the long-term behavior of PW, the linear trends of the corresponding time series were computed together with the parameters, characterizing the annual variations that appear to be the predominant harmonic, as Fig. 2 clearly exhibits. To perform such an assessment, the $\mathrm{PW_{GPS}}$ and $\mathrm{PW_{TOT}}$ time-series frequency spectra were analyzed with the Lomb–Scargle periodogram [63] to detect the significant signals, and the annual harmonic was found to be prevalent and significant at a 99.9% level. Therefore, each time series was fitted by a function of time t, having the following analytical form:

$$\mathrm{PW} = \mathrm{PW_0} + \alpha t + A \sin\left(\frac{2\pi}{T}t + \varphi\right) \tag{14}$$

where α represents the linear trend, and A is the amplitude of the variations determined by a period T and phase φ. The estimated parameters are shown in Table III with the relevant statistical errors.

The aforementioned approximations were not made for the Mario Zucchelli station because of the rather sparse data series (see Fig. 2) that are considered not sufficient to give reliable estimates of the given parameters. The GPS-derived trends given in the fourth row in Table III highlight a PW decrease at Casey (-0.03 ± 0.01 mm/year) and Mawson (-0.01 ± 0.01 mm/year). McMurdo exhibits a slight increase in PW (0.01 ± 0.01 mm/year), whereas Davis is not associated with a net variation of PW (0.00 ± 0.01 mm/year). GPS and RS observations do not exhibit consistent long-term trends: The former detects a yearly increase in PW only at McMurdo, which is not consistent with the RS results $\alpha_{\mathrm{TOT}} = 0.00 \pm 0.01$. Conversely, $\mathrm{PW_{TOT}}$ trends α_{TOT} are positive and in the range of 0.0–0.4 mm/year. The linear trends derived from the RS observations appear to be consistent, in magnitude and sign, with the predictions of several global climate models such as the Community Climate System Model 4, whose 100-year prediction for Antarctica amounts to an increase in PW of 0.1 ± 0.1 mm/year [7]. The results given in Table III demonstrate that the approximation achieved through (14) accurately defines the annual cycle in the PW variations observed by both techniques, showing that a very good agreement substantially exists between the estimates of the amplitudes, periods, and phases of GPS and RS PW time series.

V. Conclusion

The 12-year data sets of RS and GPS observations acquired in Antarctica at the coastal sites of Casey, Davis, Mawson, McMurdo, and Mario Zucchelli stations, covering the period from January 1, 1999 to December 31, 2010, were processed with the purpose of computing the PW time series and to determine their trends. For both techniques, the processing strategy was specifically developed to ensure a homogeneous and up-to-date data analysis, implementing models and parameters capable to reduce known observational or instrumental biases to a minimum (estimated to be predominantly $\leq 20\%$).

When comparing the time series of $\mathrm{PW_{GPS}}$ and $\mathrm{PW_{TOT}}$ shown in Fig. 2, the presence of systematic differences can be appreciated. There is not a consistent dry or wet bias of one technique with respect to the other. Assuming the RS results as reference, GPS appears to overestimate or underestimate the PW in varying percentages, depending on the particular site. Despite these discrepancies, the PW seasonal variations detected with the two techniques are rather consistent, as confirmed by the scatter plots and the related correlation coefficients.

The linear trends computed over PW_{GPS} and PW_{TOT} are extremely small, as can be expected in Antarctica. However, only the linear trends computed from the RS time series are consistent in sign and magnitude with the predictions of most global climate models, which foresee a small increase in PW on the order of 0.1 ± 0.1 mm/year. The trends that were computed over PW_{GPS} are consistent in magnitude but (mostly) opposite in sign, thus indicating a small decrease in PW over the 12-year period.

It is well known that careful reprocessing of GPS data is essential to obtain consistent results over long time spans. However, in Antarctica, where the values of the parameters to be determined approaches the sensitivity of the method, further investigations over longer time spans are required to assess the general PW trends derived from GPS. In such cases, the use of traditional and well-established observing techniques such as RS is essential and may represent an excellent benchmark for comparison and validation to GPS. Again, careful data processing and a conscious use of proper correction models are fundamental to obtain unbiased estimates that are valuable for a wide range of climatological applications.

ACKNOWLEDGMENT

The authors would like to thank the Meteo-Climatological Observatory, Programma Nazionale di Ricerche in Antartide (PNRA) (www.climantartide.it) for providing the radiosounding and meteorological measurements at Mario Zucchelli; the University of Wisconsin–Madison Antarctic Meteorological Research Center for the McMurdo data set (National Science Foundation Grant ANT-0537827 and Grant ANT-0838834); and the Department of Atmospheric Science, University of Wyoming for the Casey, Davis, and Mawson data sets. This work was carried out in the framework of PNRA. Fig. 1 was produced using the Generic Mapping Tools [64].

REFERENCES

[1] A. E. Dessler and S. C. Sherwood, "A matter of humidity," *Science*, vol. 323, no. 5917, pp. 1020–1021, Feb. 2009.

[2] I. M. Held and B. J. Soden, "Water vapor feedback and global warming," *Annu. Rev. Energy Environ.*, vol. 25, no. 1, pp. 441–475, Nov. 2000.

[3] T. H. Vonder Haar, J. L. Bytheway, and J. M. Forsythe, "Weather and climate analyses using improved global water vapor observations," *Geophys. Res. Lett.*, vol. 39, no. 15, Aug. 2012, Art. ID L15802.

[4] A. J. Monaghan, D. H. Bromwich, and D. P. Schneider, "Twentieth century Antarctic air temperature and snowfall simulations by IPCC climate models," *Geophys. Res. Lett.*, vol. 35, no. 7, Apr. 2008, Art. ID L07502.

[5] S. R. M. Ligtenberg, W. J. van de Berg, M. R. van den Broeke, J. G. L. Rae, and E. van Meijgaard, "Future surface mass balance of the Antarctic ice sheet and its influence on sea level change, simulated by a regional atmospheric climate model," *Clim. Dyn.*, vol. 41, no. 3/4, pp. 867–884, Aug. 2013.

[6] G. Krinner, O. Magand, I. Simmonds, C. Genthon, and J.-L. Dufresne, "Simulated Antarctic precipitation and surface mass balance at the end of the twentieth and twenty-first centuries," *Clim. Dyn.*, vol. 28, no. 2/3, pp. 215–230, Feb. 2007.

[7] R. Jacola, R. Knuteson, and S. Ackerman, "Time-to-detect trends in precipitable water vapor with varying measurement error," *J. Clim.*, vol. 27, pp. 8259–8275, Nov. 2014.

[8] M. Bevis *et al.*, "GPS meteorology: Remote sensing of atmospheric water vapor using the global positioning system," *J. Geophys. Res. Atmos.*, vol. 97, no. D14, pp. 15 787–15 801, Oct. 1992.

[9] G. V. Bennitt and A. Jupp, "Operational assimilation of GPS zenith total delay observations into the met office numerical weather prediction models," *Monthly Weather Rev.*, vol. 140, no. 8, pp. 2706–2719, Aug. 2012.

[10] S. de Haan, "Assimilation of GNSS ZTD and radar radial velocity for the benefit of very-short-range regional weather forecasts," *Quart. J. R. Meteorol. Soc.*, vol. 139, no. 677, pp. 2097–2107, Oct. 2013.

[11] J. A. Roman, R. O. Knuteson, S. A. Ackerman, D. C. Tobin, and H. E. Revercomb, "Assessment of regional global climate model water vapor bias and trends using Precipitable Water Vapor (PWV) observations from a network of Global Positioning Satellite (GPS) receivers in the U.S. Great Plains and Midwest," *J. Clim.*, vol. 25, no. 16, pp. 5471–5493, Aug. 2012.

[12] W. Rohm, Y. Yuan, B. Biadeglgne, K. Zhang, and J. L. Marshall, "Ground-based GNSS ZTD/IWV estimation system for numerical weather prediction in challenging weather conditions," *Atmos. Res.*, vol. 138, pp. 414–426, Mar. 2014.

[13] J. Wang, L. Zhang, A. Dai, T. Van Hove, and J. Van Baelen, "A near-global, 2-hourly data set of atmospheric precipitable water from ground-based GPS measurements," *J. Geophys. Res. Atmos.*, vol. 112, no. D11, Jun. 2007, Art. ID D11107.

[14] H. S. Hopfield, "Tropospheric correction of electromagnetic ranging signals to a satellite: A study of parameters," in *Electromagnetic Distance Measurement and the Influence of Atmospheric Refraction*, P. Richardus, Ed. Wageningen, The Netherlands: Netherlands Geodetic Comm., May 23–28, 1977, pp. 205–215.

[15] B. Hofmann-Wellenhof, H. Lichtenegger, and J. Collins, *Global Positioning System, Theory and Practice*, 5th ed. New York, NY, USA: Springer-Verlag, 2001, p. 382.

[16] J. L. Davis, T. A. Herring, I. I. Shapiro, A. E. E. Rogers, and G. Elgered, "Geodesy by radio interferometry—Effects of atmospheric modeling errors on estimates of baseline length," *Radio Sci.*, vol. 20, no. 6, pp. 1593–1607, Nov./Dec. 1985.

[17] P. Tregoning and T. A. Herring, "Impact of a priori zenith hydrostatic delay errors on GPS estimates of station heights and zenith total delays," *Geophys. Res. Lett.*, vol. 33, no. 23, Dec. 2006, Art. ID L23303.

[18] M. Bevis *et al.*, "GPS meteorology: Mapping zenith wet delays onto precipitable water," *J. Appl. Meteorol.*, vol. 33, no. 3, pp. 379–386, Mar. 1994.

[19] E. K. Smith and S. Weintraub, "The constants in the equation for atmospheric refractive index at radio frequencies," *Proc. IRE*, vol. 41, no. 8, pp. 1035–1037, Aug. 1953.

[20] P. Steigenberger *et al.*, "Reprocessing of a global GPS network," *J. Geophys. Res.*, vol. 111, no. B5, May 2006, Art. ID B05402.

[21] P. Steigenberger, M. Rothacher, M. Fritsche, A. Ruelke, and R. Dietrich, "Quality of reprocessed GPS satellite orbits," *J. Geodesy*, vol. 83, no. 3/4, pp. 241–248, Mar. 2009.

[22] V. Tesmer, P. Steigenberger, M. Rothacher, J. Boehm, and B. Meisel, "Annual deformation signals from homogeneously reprocessed VLBI and GPS height time series," *J. Geodesy*, vol. 83, no. 10, pp. 973–988, Oct. 2009.

[23] M. Rothacher *et al.*, "GGOS-D: Homogeneous reprocessing and rigorous combination of space geodetic observations," *J. Geodesy*, vol. 85, no. 10, pp. 679–705, Oct. 2011.

[24] P. Steigenberger *et al.*, "Comparisons of homogeneously reprocessed GPS and VLBI long time-series of troposphere zenith delays and gradients," *J. Geodesy*, vol. 81, no. 6–8, pp. 503–514, Jun. 2007.

[25] S. Vey *et al.*, "On the homogeneity and interpretation of precipitable water time series derived from global GPS observations," *J. Geophys. Res.*, vol. 114, no. D10, May 2009, Art. ID D10101.

[26] I. D. Thomas, M. A. King, P. J. Clarke, and N. T. Penna, "Precipitable water vapor estimates from homogeneously reprocessed GPS data: An intertechnique comparison in Antarctica," *J. Geophys. Res.*, vol. 116, no. D4, Feb. 2011, Art. ID D04107.

[27] R. Dach, U. Hugentobler, P. Fridez, and M. Meindl, *Bernese GPS Software Version 5.0*. Bern, Switzerland: Astron. Inst., Univ. Bern, 2007.

[28] J. Boehm, B. Werl, and H. Schuh, "Troposphere mapping functions for GPS and very long baseline interferometry from European Centre for medium-range weather forecasts operational analysis data," *J. Geophys. Res., Solid Earth*, vol. 111, no. B2, Feb. 2006, Art. ID B02406.

[29] K. Lagler, M. Schindelegger, J. Böhm, H. Krásná, and T. Nilsson, "GPT2: Empirical slant delay model for radio space geodetic techniques," *Geophys. Res. Lett.*, vol. 40, no. 6, pp. 1069–1073, Mar. 2013.

[30] Z. Altamimi, X. Collilieux, and L. Métivier, "ITRF2008: An improved solution of the international terrestrial reference frame," *J. Geodesy*, vol. 85, no. 8, pp. 457–473, 2011.

[31] D. McCarthy and G. Petit, "IERS conventions 2003," Verlag des Bundesamts für Kartographie und Geodäsie, Frankfurt, Germany, IERS Tech. Note 32, ISBN 3-89888-884-3, 2003, p. 127.
[32] E. W. Schwiderski, "On charting global ocean tides," *Rev. Geophys.*, vol. 18, no. 1, pp. 243–268, Feb. 1980.
[33] E. W. Schwiderski, "Ocean tides, part II: A hydrodynamical interpolation model," *Mar. Geodesy*, vol. 3, no. 1–4, pp. 219–255, 1980.
[34] R. Schmid, "IGS antenna working group," Int. GNSS Service, Pasadena, CA, USA, Tech. Rep., 2012, pp. 133–137. [Online]. Available: https://ftp://igs.org/pub/resource/pubs/2011_techreport.pdf
[35] T. A. Springer, *Modeling and Validating Orbits and Clocks Using the Global Positioning System* ser. Geodätisch-geophysikalische Arbeiten in der Schweiz, vol. 60. Zürich, Switzerland: Schweizerische Geodätische Kommission, 2000, p. 154.
[36] X. Yan *et al.*, "The benefit of GPS zenith delay assimilation to high-resolution quantitative precipitation forecasts: A case-study from COPS IOP 9," *Quart. J. R. Meteorol. Soc.*, vol. 135, no. 644, pp. 1788–1800, Oct. 2009.
[37] K. Boniface *et al.*, "Impact of high-resolution data assimilation of GPS zenith delay on Mediterranean heavy rainfall forecasting," *Ann. Geophys.*, vol. 27, no. 7, pp. 2739–2753, Jul. 2009.
[38] J. Saastamoinen, "Contributions to the theory of atmospheric refraction," *Bull. Géodésique (1946–1975)*, vol. 107, no. 1, pp. 13–34, Sep. 1973.
[39] P. Sarti, M. Negusini, C. Tomasi, B. Petkov, and A. Capra, "Thirteen years of integrated precipitable water derived by GPS at Mario Zucchelli Station, Antarctica," *Ann. Geophys.*, vol. 56, no. 2, 2013, Art. ID R0221.
[40] J. Kouba, "Testing of Global Pressure/Temperature (GPT) model and Global Mapping Function (GMF) in GPS analyses," *J. Geodesy*, vol. 83, no. 3/4, pp. 199–208, Mar. 2009.
[41] H. Berg, *Allgemeine Meteorologie: Einführung in die Physik der Atmosphäre*. Bonn, Germany: Dümmlers Verlag, 1948.
[42] F. Fund, L. Morel, A. Mocquet, and J. Boehm, "Assessment of ECMWF-derived tropospheric delay models within the EUREF permanent network," *GPS Solutions*, vol. 15, no. 1, pp. 39–48, Jan. 2011.
[43] P. Steigenberger, J. Boehm, and V. Tesmer, "Comparison of GMF/GPT with VMF1/ECMWF and implications for atmospheric loading," *J. Geodesy*, vol. 83, no. 10, pp. 943–951, Oct. 2009.
[44] J. K. Luers and R. E. Eskridge, "Temperature corrections for the VIZ and Vaisala radiosondes," *J. Appl. Meteorol.*, vol. 34, no. 6, pp. 1241–1253, Jun. 1995.
[45] J. K. Luers, "Temperature error of the Vaisala RS90 radiosonde," *J. Atmos. Ocean. Technol.*, vol. 14, no. 6, pp. 1520–1532, Dec. 1997.
[46] C. Tomasi *et al.*, "Mean vertical profiles of temperature and absolute humidity from a 12-year radiosounding data set at Terra Nova Bay (Antarctica)," *Atmos. Res.*, vol. 71, no. 3, pp. 139–169, Aug./Sep. 2004.
[47] P. M. Rowe, L. M. Miloshevich, D. D. Turner, and V. P. Walden, "Dry bias in Vaisala RS90 radiosonde humidity profiles over Antarctica," *J. Atmos. Ocean. Technol.*, vol. 25, no. 9, pp. 1529–1541, Sep. 2008.
[48] L. M. Miloshevich, A. Paukkunen, H. Vömel, and S. J. Oltmans, "Development and validation of a time-lag correction for Vaisala radiosonde humidity measurements," *J. Atmos. Ocean. Technol.*, vol. 21, no. 9, pp. 1305–1327, Sep. 2004.
[49] L. M. Miloshevich *et al.*, "Absolute accuracy of water vapor measurements from six operational radiosonde types launched during AWEX-G and implications for AIRS validation," *J. Geophys. Res. Atmos.*, vol. 111, no. D9, May 2006, Art. ID D09S10.
[50] J. Wang *et al.*, "Corrections of humidity measurement errors from the Vaisala RS80 radiosonde-application to TOGA COARE data," *J. Atmos. Ocean. Technol.*, vol. 19, no. 7, pp. 981–1002, Jul. 2002.
[51] D. D. Turner *et al.*, "Dry bias and variability in Vaisala RS80-H radiosondes: The ARM experience," *J. Atmos. Ocean. Technol.*, vol. 20, no. 1, pp. 117–132, Jan. 2003.
[52] L. M. Miloshevich, H. Vömel, D. N. Whiteman, and T. Leblanc, "Accuracy assessment and correction of Vaisala RS92 radiosonde water vapor measurements," *J. Geophys. Res. Atmos.*, vol. 114, no. D11, Jun. 2009, Art. ID D11305.
[53] L. M. Miloshevich, H. Vömel, A. Paukkunen, A. J. Heymsfield, and S. J. Oltmans, "Characterization and correction of relative humidity measurements from Vaisala RS80-A radiosondes at cold temperatures," *J. Atmos. Ocean. Technol.*, vol. 18, no. 2, pp. 135–156, Feb. 2001.
[54] K. E. Cady-Pereira *et al.*, "Improved daytime column-integrated precipitable water vapor from Vaisala radiosonde humidity sensors," *J. Atmos. Ocean. Technol.*, vol. 25, no. 6, pp. 873–883, Jun. 2008.
[55] D. M. Murphy and T. Koop, "Review of the vapour pressures of ice and supercooled water for atmospheric applications," *Q. J. R. Meteorol. Soc.*, vol. 131, no. 608, pp. 1539–1565, 2005.
[56] C. Tomasi, B. H. Petkov, and E. Benedetti, "Annual cycles of pressure, temperature, absolute humidity and precipitable water from the radiosoundings performed at Dome C, Antarctica, over the 2005–2009 period," *Antarctic Sci.*, vol. 24, pp. 637–658, Dec. 2012.
[57] J. A. Goff and S. Gratch, "Low-pressure properties of water from −160 to 212 F," in *Proc. Trans. 52nd Annu. Meet. Amer. Soc. Heating Ventilating Eng.*, New York, NY, USA, 1946, vol. 52, pp. 95–122.
[58] D. Bolton, "The computation of equivalent potential temperature," *Mon. Weather Rev.*, vol. 108, no. 7, pp. 1046–1053, Jul. 1980.
[59] C. Tomasi, B. Petkov, E. Benedetti, L. Valenziano, and V. Vitale, "Analysis of a 4 year radiosonde data set at Dome C for characterizing temperature and moisture conditions of the Antarctic atmosphere," *J. Geophys. Res. Atmos.*, vol. 116, no. D15, Aug. 2011, Art. ID D15304.
[60] C. Tomasi *et al.*, "Monthly mean vertical profiles of pressure, temperature and water vapour volume mixing ratio in the polar stratosphere and low mesosphere from a multi-year set of MIPAS-ENVISAT limb-scanning measurements," *J. Atmos. Sol. Terrestrial Phys.*, vol. 73, no. 16, pp. 2237–2271, Oct. 2011.
[61] S. Vey *et al.*, "Validation of precipitable water vapor within the NCEP/DOE reanalysis using global GPS observations from one decade," *J. Clim.*, vol. 23, no. 7, pp. 1675–1695, Apr. 2009.
[62] T. Ning, R. Haas, G. Elgered, and U. Willén, "Multi-technique comparisons of 10 years of wet delay estimates on the west coast of Sweden," *J. Geodesy*, vol. 86, no. 7, pp. 565–575, Jul. 2012.
[63] J. D. Scargle, "Studies in astronomical time series analysis. II—Statistical aspects of spectral analysis of unevenly spaced data," *Astrophys. J.*, vol. 263, pp. 835–853, Dec. 1982.
[64] P. Wessel, W. H. F. Smith, R. Scharroo, J. Luis, and F. Wobbe, "Generic Mapping Tools: Improved version released," *EOS, Trans. Amer. Geophys. Union*, vol. 94, no. 45, pp. 409–410, Nov. 2013.

Monia Negusini (M'14) received the M.S. degree in astronomy and the Ph.D. degree in geophysics from the University of Bologna, Bologna, Italy, in 1994 and 2005, respectively.

Since 2001, she has been working as a Researcher with the Institute of Radio Astronomy, Italian National Institute of Astrophysics (INAF), Bologna, Italy. She is the author or coauthor of 50 scientific papers published on international journals and international and national meeting proceedings. Her research focuses on the use and integration of space geodetic observations for tropospheric water vapor studies, particularly using Very Long Baseline Interferometry (VLBI) and GPS data. Crustal deformation in Victoria Land (Antarctica) is investigated using GPS, and the evolution of Mt. Etna (Italy), using GPS and VLBI data.

Dr. Negusini is the Chair of Work Package 2 [lower atmosphere delay in global navigation satellite system (GNSS)-based systems (water vapor reconstruction, etc.)] of the GNSS Research and Application for Polar Environment (GRAPE) Expert Group within the Scientific Committee on Antarctic Research. She is an Associate Member of the International VLBI Service for Geodesy and Astrometry (IVS) and is the INAF Contact Point.

Boyan H. Petkov received the M.S. degree in physics from Sofia University "St. Kliment Ohridski," Sofia, Bulgaria, in 1985 and the Ph.D. degree in atmospheric physics from the Hydrometeorological University, St. Petersburg, Russia, in 1990.

Since 2002, he has been working with the Institute of Atmospheric Sciences and Climate (ISAC), Italian National Research Council (CNR), Bologna, Italy. The main field of his activity is the interaction between solar radiation and atmospheric constituents, particularly the study of the thermodynamical air conditions through the analysis of radiosounding data, the conditions of which are very important for the radiative processes occurring in the Earth's atmosphere and their effects on the climate.

Pierguido Sarti received the M.S. degree in physics and the Ph.D. degree in topography and geodesy (with a thesis focused on the use of Very Long Baseline Interferometry and Global Positioning System techniques for atmospheric water vapor retrieval) from the University of Bologna, Bologna, Italy, in 1997 and 2000, respectively.

In 2001, he held a research position with the Italian National Research Council (CNR), and since 2005, he has been a Researcher with the Institute of Radio Astronomy, Italian National Institute of Astrophysics (INAF), Bologna, Italy. He took part in four Italian Antarctic expeditions and was twice in the Arctic, at the Ny Alesund scientific facility in Svalbard Islands. He is the author of more than 60 scientific papers in the field of geodesy. His main scientific interests include the atmospheric sensing in polar regions with space geodetic radio techniques and the colocations of geodetic sensors.

Dr. Sarti chaired the International Earth Rotation and Reference Systems Service Working Group on Colocations of Space Geodetic Instruments from 2009 to 2013.

Claudio Tomasi received the M.S. degree in physics from the University of Bologna, Bologna, Italy, in 1970.

From 1970 to 1991, he worked as a Researcher with the Italian National Research Council (CNR), Bologna, Italy, where he then worked as the Director of research from 1991 to 2006. He retired in April 2006, but he continues his research activity as an Associate Researcher with the Institute of Atmospheric Sciences and Climate (ISAC), CNR. From 2006 to 2008, he was a Partner of the Climate Impacts of Short-Lived Pollutants in the Polar Region (CLIMSLIP) Project, in which studies have been developed on the optical characteristics of polar aerosols through ground-based and shipborne sun-photometer measurements, Lidar system observations, and remote sensing measurements with satellite sensors. He is the author of more than 150 papers in the field of atmospheric sciences, which were published in international peer-reviewed journals and international conference proceedings, and of more than 160 articles published in national journals, technical reports, scientific memos, and books. He is currently studying the direct radiative forcing effects induced by aerosols on the surface–atmosphere system and their dependence on aerosol optical thickness, with particular attention paid to the aerosol optical parameters and the bidirectional surface reflectance properties in the Po valley (Italy) and in polar regions, including the preparation of new correction procedures for the analysis of radiosonde data collected at Arctic and Antarctic sites.